North Atlantic jet stream projections in the context of the past 1,250 years

Matthew B. Osman[a,b,1], Sloan Coats[c], Sarah B. Das[d], Joseph R. McConnell[e], and Nathan Chellman[e]

[a]Massachusetts Institute of Technology/Woods Hole Oceanographic Institution Joint Program in Oceanography/Applied Ocean Sciences and Engineering, Woods Hole, MA 02543; [b]Department of Geosciences, University of Arizona, Tucson, AZ 85721; [c]Department of Earth Sciences, University of Hawaii, Honolulu, HI 96822; [d]Department of Geology and Geophysics, Woods Hole Oceanographic Institution, Woods Hole, MA 02543; and [e]Division of Hydrologic Sciences, Desert Research Institute, Reno, NV 89512

Edited by Dim Coumou, Vrije Universiteit Amsterdam, Amsterdam, The Netherlands, and approved July 21, 2021 (received for review March 2, 2021)

Reconstruction of the North Atlantic jet stream (NAJ) presents a critical, albeit largely unconstrained, paleoclimatic target. Models suggest northward migration and changing variance of the NAJ under 21st-century warming scenarios, but assessing the significance of such projections is hindered by a lack of long-term observations. Here, we incorporate insights from an ensemble of last-millennium water isotope–enabled climate model simulations and a wide array of mean annual water isotope ($\delta^{18}O$) and annually accumulated snowfall records from Greenland ice cores to reconstruct North Atlantic zonal-mean zonal winds back to the 8th century CE. Using this reconstruction we provide preobservational constraints on both annual mean NAJ position and intensity to show that late 20th- and early 21st-century NAJ variations were likely not unique relative to natural variability. Rather, insights from our 1,250 year reconstruction highlight the overwhelming role of natural variability in thus far masking the response of midlatitude atmospheric dynamics to anthropogenic forcing, consistent with recent large-ensemble transient modeling experiments. This masking is not projected to persist under high greenhouse gas emissions scenarios, however, with model projected annual mean NAJ position emerging as distinct from the range of reconstructed natural variability by as early as 2060 CE.

North Atlantic | jet stream | ice core | Greenland | climate change

Variations in the intensity and position of the North Atlantic jet stream (NAJ)—currents of strong prevailing westerly winds situated over the midlatitudes—play a critical role in modulating North American and European weather and climate, transport, commerce, and ecosystems (1–3). The NAJ arises principally as a consequence of equator-to-pole temperature gradients that, on a global scale, drive westerly winds through a balance between the associated pressure gradient that accelerates warm equatorial airmasses poleward and the eastward deflection of those airmasses due to Earth's rotation. In the midlatitudes, these winds are often described as "eddy-driven" due to the central role of baroclinic eddies (extratropical cyclones) in maintaining the resultant mean westerly flow over the depth of the troposphere (4).

During the past two centuries, near-surface equator-to-pole temperature gradients have decreased markedly due to enhanced Arctic warming (5). Given the association between midlatitude temperature gradients and the frequency, position, and intensity of baroclinic eddy formation (4), considerable effort has been spent attempting to isolate an anthropogenically forced signal in the NAJ (6–11). The conventional approach involves the use of observations that span the daily to weekly ("synoptic") timescales over which eddy activity is largest, and these observations have hinted at an increase in the frequency of extreme storms over recent decades (1, 7). However, the mechanism(s) linking such changes to anthropogenic forcing of the NAJ remain widely debated (10, 12); one hypothesis holds that intensified atmospheric blocking has produced a weakening (i.e., stagnation) of NAJ intensity and (or) enhanced north–south deviations in its position (7), although weakening of the stratospheric polar vortex (13) or the "trapping" of large-scale atmospheric waves (6, 8) (quasiresonant amplification) have also been hypothesized.

Despite the central focus to date on the synoptic-scale NAJ, significant, societally relevant NAJ variations also occur from interannual to centennial timescales (14–16). While it is difficult to characterize NAJ variations on these timescales from the limited observational record, apart from a recent tree ring–based, August-only three-century reconstruction of NAJ position (6) (and notwithstanding reconstructions of the NAJ position-related North Atlantic Oscillation, or NAO [refs. 9 and 17–19 and see *SI Appendix*]), there are to our knowledge no reconstructions of the NAJ prior to the mid-19th century. This hinders our ability to contextualize both contemporary observations (14, 16) and model-derived projections of future NAJ changes (20, 21) and understand long-term drivers of NAJ variability.

Here, we use measurements of two meteoric proxies, the annually resolved oxygen isotopic composition of precipitation ($\delta^{18}O$; *Materials and Methods*) as well as the amount of annually accumulated snowfall deposited across Greenland, to reconstruct past variations in the NAJ. We focus on the low-altitude, mean-annual component of the NAJ due to its connection to the Atlantic storm track and hence relevance to people and ecosystems in North America and Europe (1–3, 22). Herein, we first

Significance

The North Atlantic jet stream impacts North American and European societies and is expected to be influenced by ongoing 21st-century warming. To better contextualize recently observed and model-projected jet stream changes, long-term records are required. We use insights from a state-of-the-art water isotope–enabled climate model and a compilation of ice-core records from Greenland to reconstruct mean annual North Atlantic jet stream changes back to the 8th century CE. Our reconstruction suggests that observed jet stream variations are consistent with natural variations, despite dramatic warming across recent decades. Under unabated future warming, however, a progressive migration of the jet stream northward is projected to render it distinct from natural variability by 2060 CE.

Author contributions: M.B.O. and S.C. designed research; M.B.O., S.C., S.B.D., J.R.M., and N.C. performed research; M.B.O. analyzed data; and M.B.O. and S.C. wrote the paper.

The authors declare no competing interest.

This article is a PNAS Direct Submission.

[1]To whom correspondence may be addressed. Email: mattosman@arizona.edu.

This article contains supporting information online at https://www.pnas.org/lookup/suppl/doi:10.1073/pnas.2104105118/-/DCSupplemental.

Published September 13, 2021.

provide a descriptive framework for the NAJ based on observations that—when combined with modeling-based insights—enables robust prediction of the ideal locations of NAJ proxies. We then isolate two unique modes of variability from Greenland ice-core proxies that, together, enable skillful reconstruction of the NAJ back to the 8th century CE. We close by discussing our reconstruction in the context of long-term changes, influences, and potential past and future societal implications of the changing NAJ.

NAJ Characterization and Proxy Development

Conventional analyses of the NAJ have their basis in two primary frameworks, using "geometric" or "statistic" approximations, respectively (14, 16, 20). Both frameworks are premised on a one-dimensional representation of North Atlantic zonal winds, produced by zonally averaging mean-annual near-surface (925 to 700 hPa) zonal winds over the region 60°W-0°E, 15-75°N (Fig. 1*A*)—hereinafter the North Atlantic zonal wind profile—in this case using two climate reanalyses: the National Oceanic and Atmospheric Administration (NOAA) and ERA 20th Century reanalysis datasets (23, 24) (NOAA20C and ERA20C; *Materials and Methods*). In this zonal-mean representation, the NAJ manifests as a zonal wind speed "bulge" centered about the midlatitudes (Fig. 1*A*); herein, NAJ intensity and position are geometrically assessed via year-to-year changes in maximum speed and the corresponding latitudinal alignment of that maximum, respectively (16, 20) (Fig. 1). In contrast, the statistic framework decomposes the same North Atlantic zonal wind profile into a set of orthogonal "modes" of spatiotemporal variability using principal component analysis (PCA). Here, the leading two modes (hereinafter Jet-PC1 and -PC2) explain 85% of the observed variance, with Jet-PC1 describing the meridional "wobbling" of the NAJ, and Jet-PC2 its zonal "pulsation" (20) (Fig. 1*B*).

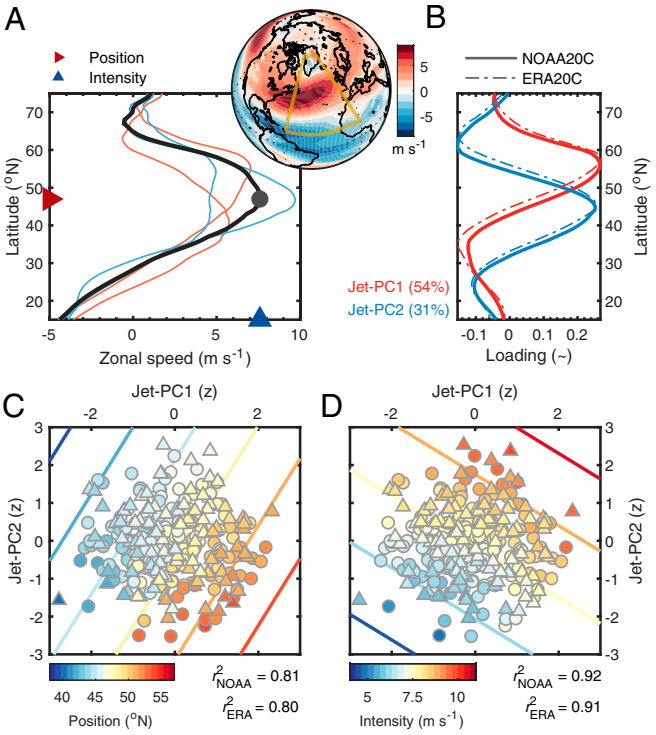

Fig. 1. Relationship between geometric and statistic NAJ descriptions. (*A*) Geometric description of the North Atlantic zonal wind profile, created by zonally averaging mean annual near-surface zonal wind speeds over the North Atlantic (yellow boxed region on inset globe; *Materials and Methods*). Blue and red lines correspond to years with the maximum and minimum intensity (blue) and position (red) indices from the NOAA20C product, while the globe inset shows climatological mean annual near-surface zonal winds (1900 to 2015 CE). (*B*) Statistic description (14), showing the leading two modes of variability for the North Atlantic zonal wind profile (Jet-PC1 and -PC2). (*C* and *D*) Bilinear prediction of position (*C*) and intensity (*D*) from Jet-PC1 and -PC2 (circles and triangles denote NOAA20C and ERA20C data, respectively).

Contrasting the two frameworks (Fig. 1 *A* and *B*), the relative merits of each are apparent: The geometric approach is intuitive and thus societally relevant, but at cost of integrating useful information on the full North Atlantic zonal wind profile (Fig. 1*B*). The statistic framework has the added advantage of being particularly amenable to established climate reconstruction methodologies (e.g., ref. 25 and see *SI Appendix*). Despite any differences, strong correlation exists between observations of Jet-PC1 with NAJ position (63 to 70% variance explained; *SI Appendix*, Fig. S1*A*) and Jet-PC2 with NAJ intensity (54 to 78% variance explained; *SI Appendix*, Fig. S1*C*). Extending these insights further, even greater proportions of the NAJ position and intensity variances are captured, at 80% and >90%, respectively, by combining Jet-PC1 and -PC2 as multilinear predictors for both (Fig. 1 *C* and *D* and *SI Appendix*, Fig. S1 *B* and *D*). This latter finding is salient: If robust signals of Jet-PC1 and -PC2 can be extracted from climatic proxies, then this will allow for reconstruction of NAJ position and intensity as well (16).

To enable insight into the optimal locations of NAJ proxies, we leverage the statistic framework by quantifying the spatiotemporal covariance of Jet-PC1 and -PC2 against atmospheric pressure, annually accumulated precipitation (which closely approximates the annually accumulated snowfall proxies), and precipitation-weighted δ^{18}O deposition using reanalyses (23) and climate model simulations. For the latter, we incorporate a suite of state-of-the-art model runs from the isotope-enabled Community Earth System Model Last Millennium Ensemble (26, 27) (iCESM-LME), which simulate the variables [principally, the abundance of meteoric water isotopes (27)], timescales (up to centennial), and time period (the last millennium) of interest (*Materials and Methods*). Our results, encapsulated in *SI Appendix*, Fig. S2 and described at length in *SI Appendix*, indicate that both mean annual δ^{18}O and annually accumulated precipitation variations deposited and stored as glacial ice across Greenland contain robust spatial signatures of Jet-PC1 and -PC2 (*SI Appendix*, Fig. S2 *C* and *D*): For δ^{18}O, Jet-PC1 manifests as strong, positively correlated anomalies across Greenland, whereas Jet-PC2 invokes a comparably weak north–south trending δ^{18}O-anomaly dipole. By contrast, Jet-PC2 produces a particularly strong annually accumulated precipitation imprint across south-central Greenland. Regardless of any iCESM biasing of δ^{18}O and precipitation over Greenland (27), the unique sensitivities of δ^{18}O to Jet-PC1 and precipitation to Jet-PC2 imply both Greenlandic proxies are needed to constrain the NAJ.

With this as motivation, we combine an initial 29 mean annual δ^{18}O and 16 annually accumulated snowfall ice-core records from sites spanning the Greenland Ice Sheet (GrIS) and its glaciated peripheries (*SI Appendix*, Fig. S3 and Table S1). We incorporate a probabilistic PCA methodology in order to isolate the dominant modes of GrIS variability and also to narrow down our compilation to a more coherent subset of $n = 41$ records (*SI Appendix*). Consistent with iCESM predictions (*SI Appendix*, Fig. S2*C*), our analysis shows the leading proxy mode, GrIS-PC1, loads positively across all Greenland sites while explaining ~17 to 25% of the proxy variance (Fig. 2*A*). This mode has been identified in previous GrIS ice-core compilations (17, 19, 28), wherein it has been interpreted in the context of the NAO. Our results support this interpretation, with GrIS-PC1 exhibiting strongly significant correlations ($r = 0.47$ to 0.49, $P < 0.001$, $n = 101$ y; *SI Appendix*) with both Jet-PC1 and the NAO

(Fig. 2*A* and *SI Appendix*, Fig. S4) during the period of overlap with the reanalyses. Adding to these prior analyses, our compilation also reveals a second proxy mode (GrIS-PC2) that is significant at the $P < 0.001$ level (Fig. 2*B*). GrIS-PC2 explains ~9 to 15% of the proxy variance (Fig. 2*B*) and shows significant correlation ($r = 0.35$, $P < 0.01$; $n = 101$ y) with Jet-PC2 (Fig. 2*D* and *SI Appendix*, Fig. S4). This mode illuminates a northern-to-southern-trending dipole in site loadings, once again corroborating iCESM predictions (*SI Appendix*, Fig. S2*C*). Together the modes explain ~30 to 40% of the annual GrIS proxy variance, a considerable proportion given local-scale noise inherent to meteoric proxies. Critically, our ice-core data also confirm iCESM suggestions that both δ^{18}O and annually accumulated accumulation records are necessary to isolate both signals of the NAJ (Fig. 2 *C* and *D*).

Last-Millennium Reconstruction of the NAJ

Isolation of Jet-PC1 and -PC2 from our GrIS compilation allows us to reconstruct the NAJ beyond the observational era, provided time stationarity in the underlying statistical relationships linking our GrIS compilation to the NAJ. We directly calibrate the GrIS compilation to both the NOAA20C- and ERA20C-derived North Atlantic zonal wind profiles during the overlapping time period (1900 to 2000 CE). Subsequent stepwise cross-validation tests (*SI Appendix*, Table S2) revealed significant ($P < 0.10$) predictive power across all reconstruction nests back to 747 CE (beyond which a robust GrIS-PC2 signal can no longer be isolated; Fig. 3 *A* and *B*), while ensuring that at least two proxy modes were used (Fig. 1 *C* and *D*). Independent pseudoproxy experiments using the iCESM-LME, as well as seasonal bias and sensitivity testing of our proxies, further confirmed the conceptual, statistical, and temporal integrity of the reconstructions across a broad array of internal variability and external climatic forcing conditions during the last millennium (*SI Appendix*, Figs. S5 and S6 and Table S2).

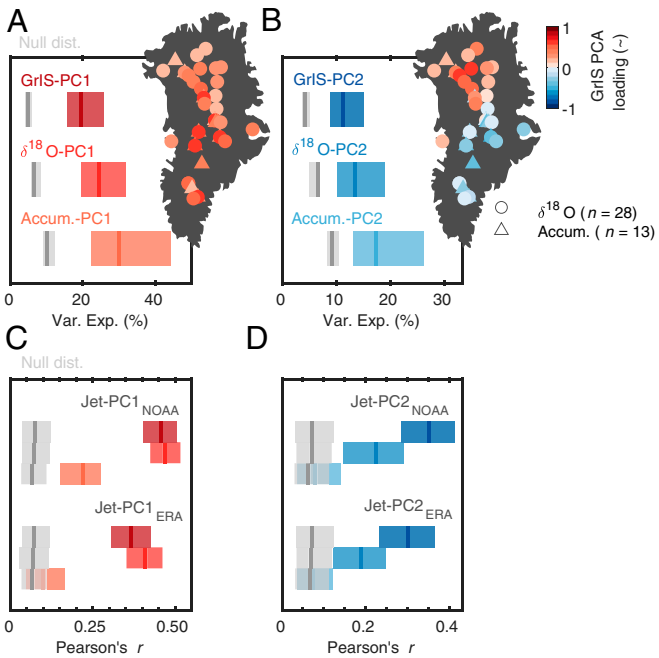

Fig. 2. Extraction of NAJ signals from Greenlandic ice-core proxies. (*A*) Variance explained by GrIS-PC1 (*Top*), δ^{18}O-PC1 (*Middle*), and annually accumulated snowfall (Accum.)-PC1 (*Bottom*) following bootstrap analysis. Shaded bands represent the 2.5th to 97.5th percentile range and the bold line the 50th percentile. Also shown are null distributions of explained variance (gray) following 1,000 PCAs conducted using power-spectrum-preserving surrogate datasets, revealing each PC1 series to be significant at the $P < 0.001$ level (*SI Appendix*). Map inset shows the GrIS-PC1 spatial loading pattern (unit normalized). (*B*) As in *A*, but for GrIS-PC2. (*C*) Correlation analyses for all three PC1 time series (GrIS-, δ^{18}O-, Accum.-PC1) vs. Jet-PC1 following 1,000 bootstrap correlation tests for the overlapping interval AD 1900 to 2000. Null distributions represent 1,000 correlations conducted using pseudorandom surrogate time series. (*D*) As in *C*, but for all three PC2 time series vs. Jet-PC2. Note that only GrIS-PC1 and PC2 (i.e., combining δ^{18}O and annually accumulated accumulation records) allow significant extraction of both Jet-PC1 and -PC2 signals.

Our reconstruction of the North Atlantic zonal wind profile enables complementary extraction of the "geometric" NAJ position and intensity metrics. Despite neither NAJ position nor intensity being direct reconstruction targets, each is 1) significant at the >99% confidence level over the full reconstruction period (Fig. 3*B*), 2) linearly independent of each other (accordant with observations, i.e., $r^2 \leq 0.03$; $n = 1{,}254$ y), and 3) strongly consistent whether calibrated to NOAA20C or ERA20C ($r^2 > 0.9$; $n = 1{,}254$ y), lending added merit to our North Atlantic zonal wind profile reconstruction. Both NAJ position and intensity illuminate marked interannual-scale variations across the last millennium ranging from 40.6° to 53.9°N and 5.4 to 10.6 m·s^{-1} (Fig. 3 *C* and *D*).

By greatly extending the observational record of NAJ variability, our reconstruction provides insights into decadal and longer timescale variability in the NAJ during the last 13 centuries. Notwithstanding the possibility for obscuring of seasonal-specific relationships by our annual mean reconstruction (28), we test the influence of external forcing on the NAJ via spectral decomposition of its reconstructed position and intensity metrics. For the former, we find evidence of energy concentrated near the 11-y period (*SI Appendix*, Fig. S7*A*). At face value this implies support for prior suggestions [based primarily on post-mid-20th century observations (29) and limited modeling experiments (30)] that NAJ position is modulated by the solar irradiance cycle. Nevertheless, when comparing NAJ position directly against reconstructed indices of total solar irradiance (31) (TSI; 850 to 2000 CE) we find little evidence of systematic TSI–NAJ coherence prior to the mid-20th century across annual mean timescales, raising the possibility that the significant 11-y periodicity we observe may instead arise as an artifact of internally generated, quasi-decadal variability (30, 32). Examination of NAJ intensity, in turn, shows strongest variance associated with lower frequency 50- to 70-y spectral bands (*SI Appendix*, Fig. S7*B*), indicating possible interplay between NAJ intensity and Atlantic Multidecadal Variability (AMV), which is also associated with these timescales (33, 34). Assuming as much, our findings corroborate ref. 35, who, using 20th-century reanalysis data, showed positive covariation between blocking frequency, which is tightly coupled to NAJ intensity (15), and sea-surface temperatures over the eastern- and northern-Atlantic sector, typical AMV centers of action (15). Finally, neither our NAJ position nor intensity reconstructions show any persistent changes during the Medieval Warm Period [*ca*. 950 to 1250 CE (18)], a period of lessened volcanic activity (36) and relatively high solar irradiance (31). More generally, unlike prior North Atlantic climate reconstructions (for example, of the NAO, cf. refs. 19 and 28), we find only weak evidence for systematic NAJ–volcanic linkages during the last millennium (*SI Appendix*, Fig. S8 *A* and *B*), rendering this an important topic for future study (see *SI Appendix*).

Given that between 10 and 50% of the observed variance in annual precipitation and temperature across eastern North America and western Europe can be explained by the NAJ (22) (*SI Appendix*, Fig. S9), it is informative to contextualize reconstructed NAJ variability with the historical record. For example, two of the most detrimental famines in Ireland and central-north England occurred during the years 1728 and 1740 CE; the latter, in particular, claimed the lives of nearly half a million individuals

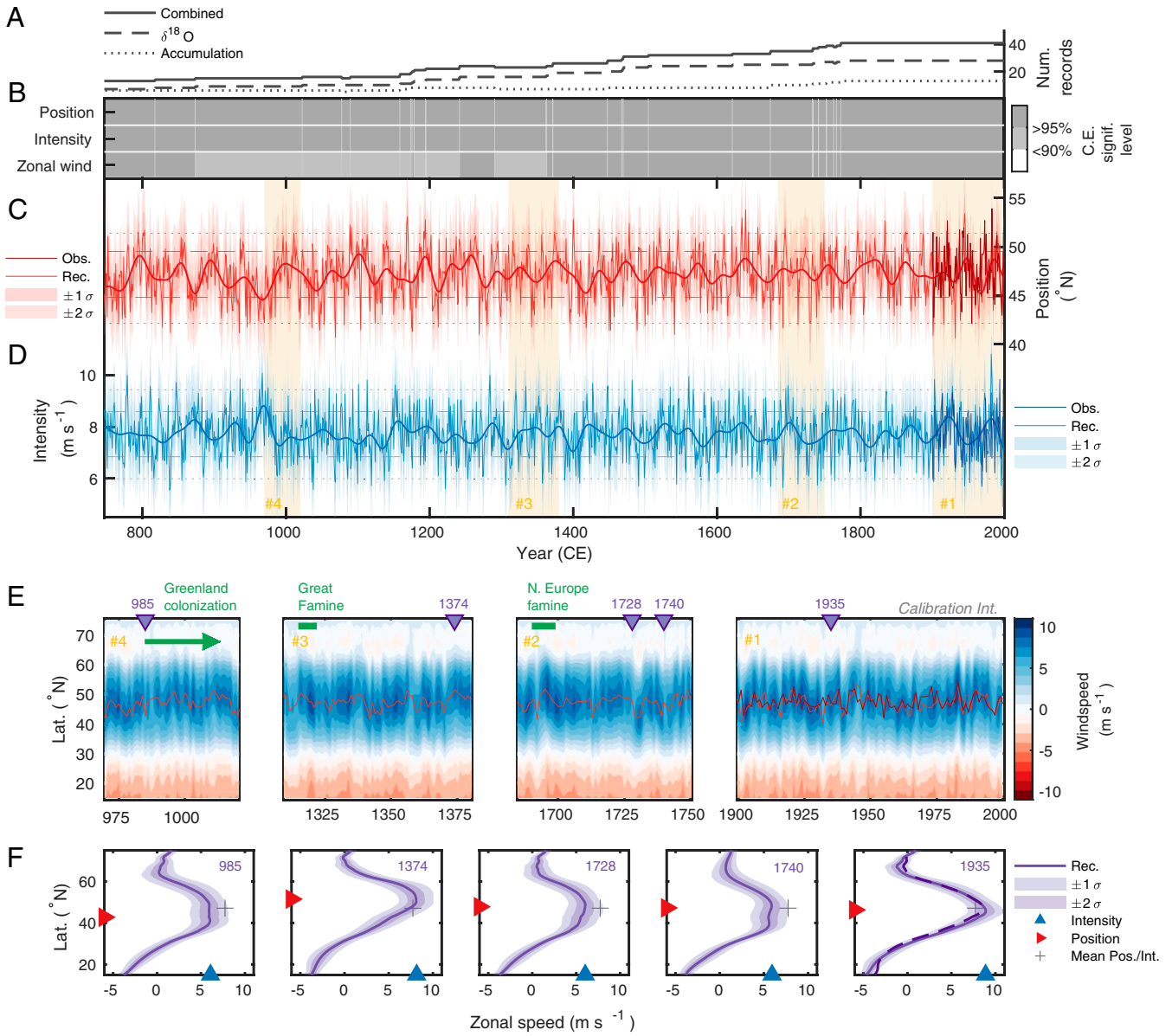

Fig. 3. Skillful reconstruction of the North Atlantic zonal wind profile during the last millennium. (*A*) Availability of Greenland δ^{18}O and annually accumulated snowfall ice-core records over time. (*B*) Coefficient of efficiency (C.E.) significance levels for NAJ position, intensity, and the North Atlantic zonal wind profile for all nested models. Note that all nests have C.E. values greater than 0, signifying skill above climatology in the reconstruction. (*C*) NAJ position (red) and (*D*) intensity (blue) derived from the North Atlantic zonal wind profile reconstruction. The dark lines show NAJ position and intensity from the NOAA20C reanalysis, and the bold smooth lines show 30-y low-pass-filtered time series. Underlying dashed and dotted levels show the $\pm1\sigma$ range and the middle 95% range, respectively. (*E*) Hovmöller diagrams of the North Atlantic zonal wind profile for four selected time periods; note that observed and reconstructed NAJ positions are illuminated as dark (right panel) and light (all panels) red lines, respectively. Purple arrows at top of *E* denote years shown in *F*. (*F*) Selected annual snapshots of the North Atlantic zonal wind profile, as discussed in the text. All results shown are calibrated to the NOAA20C reanalysis (23) over 1900 to 2000 CE.

(37). These years, reported by historical documents and nearby temperature gauges as unusually cold (38), entailed widespread failure in staple potato and grain harvests during a nearly year-long absence of rainfall. From Fig. 3 *E* and *F* we see that both years were associated with an unusually low-intensity NAJ (<3rd percentile; cf. *SI Appendix*, Fig. S9). Likewise, widespread famine recorded across northern Europe during the 1690s appears to have occurred against the backdrop of a decade of NAJ extremes: An anomalously low-intensity, southward-shifted NAJ during the early 1690s (years described as anomalously cold and dry across Fennoscandia) was proceeded by an extreme northward shift in the NAJ in 1695 CE, coincident with the Sabancaya, Peruvian eruption [changes accompanied by contrastingly cold and wet conditions recorded across Fennoscandia (39)]. Despite analysis of individual years' being challenged by dating uncertainties (particularly further back in time), a prolonged 2-y period of drought and famine reported across the Mediterranean (40) during 1374 to 1375 CE is also found to conspicuously align with a highly anomalous northward shift (>99th percentile) of the NAJ. A final historical period of interest is the initial exploration and subsequent three centuries of successful colonization of southwestern Greenland by the Norse at the turn of the last millennium (41) (*ca.* 985 CE). This coincided with a prolonged period of lower-than-average NAJ intensity (roughly 60%

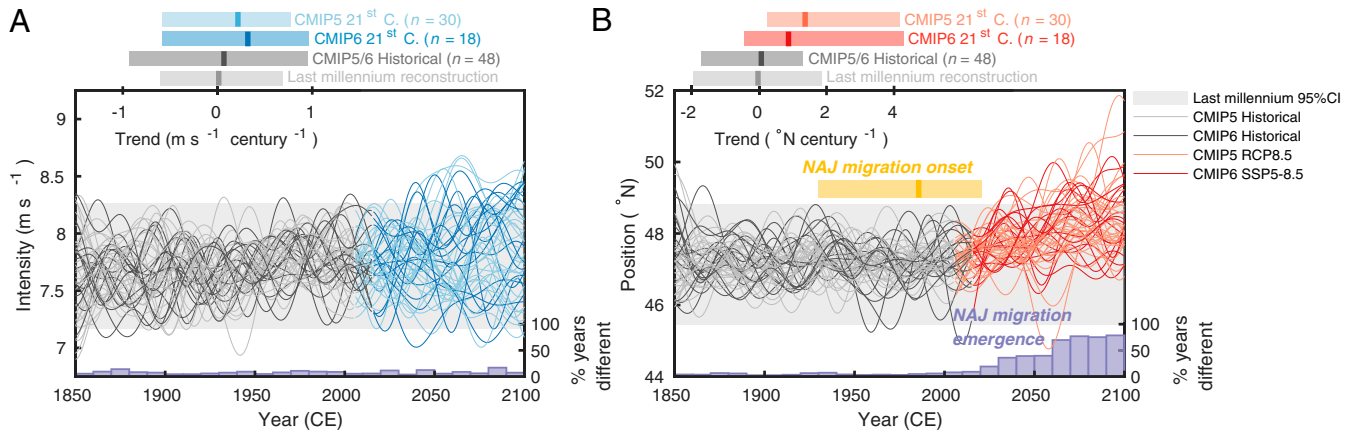

Fig. 4. Projected NAJ intensity and position changes under high-emissions scenarios. CMIP-modeled mean annual NAJ intensity (*A*) and position (*B*) for the RCP8.5 and SSP5-8.5 emissions scenarios, smoothed for visualization at 30-y low-pass resolution. All CMIP5 and CMIP6 model runs are recentered to have the same mean NAJ intensity and position as the NOAA20C reanalysis between 1900 and 2000 CE. Shown for comparison (light gray shading) is the reconstructed range (95% CI) of (30-y low-pass) NAJ intensity and position during the last 13 centuries. The cross-model onset timing for sustained, significant ($P < 0.05$) northward NAJ migration (*SI Appendix*) is shown in yellow (median and 95% CI range; $n = 48$) in *B*. Projected 21st century NAJ position and intensity trends (median and 95% CI range) are shown relative to the last millennium (all 100-y periods) and CMIP-historical period (1850 to 2005 CE), at the top. Shown at the bottom in purple is the percent of years per decade whose CMIP-modeled NAJ position and intensity are significantly different ($P < 0.05$) than the NAJ position and intensity range exhibited by the reconstruction.

of years during the late 9th to 11th centuries; Fig. 3 *E* and *F*), which could help to explain a regional rise in temperatures (*SI Appendix*, Fig. S9*F*) during these decades as recorded by local sediment proxies (42).

Contextualizing Historical and Future NAJ Projections

By extending the scope of a recent three-century, eastern-Atlantic (10-30°W) NAJ position reconstruction by ref. 6, our 13-century reconstruction allows us to test their conclusion that industrial era anthropogenic warming and weakening of the poleward temperature gradient (5) has recently led (*ca*. late 20th century) to enhanced variability in the position of the NAJ (6, 7). Although several nontrivial differences between the reconstruction target of ref. 6 and our own (August vs. mean annual, high vs. low altitude) as well as methodological discrepancies hinder a straightforward comparison (cf. *SI Appendix*, Fig. S10 and *SI Appendix*), our reconstruction does not support the notion that variability in NAJ position during recent decades is overtly exceptional across a longer 13-century context (*SI Appendix*, Fig. S7*C*). The same is true of NAJ intensity, and thus the available evidence suggests that an annual mean anthropogenic NAJ signal has not yet emerged from the range of variations expected from naturally driven processes alone, although we acknowledge that our use of annually averaged data could be masking underlying long-term, seasonal-specific trends (7, 12, 14, 20).

Given our result that annual mean NAJ position and intensity has not yet emerged from natural variability, we contextualize projected future shifts in the NAJ (20, 21) using model output from phases 5 and 6 of the Coupled Model Intercomparison Projects (43, 44) (CMIP5 and CMIP6) under the high-emissions Representative Concentration Pathway 8.5 (RCP8.5) and Shared Socioeconomic Pathway #5 8.5 (SSP5-8.5) future climate scenarios (see *Materials and Methods*). Following minimal (mean-bias) adjustments of the modeled NAJ position and intensity metrics to achieve consistency with our reconstruction (*SI Appendix*, Table S3 and *Materials and Methods*), we compare natural variability in the NAJ to the emergence of an anthropogenically forced signal. Our results show that models do not consistently project shifts in NAJ intensity in the future (Fig. 4*A* and ref. 20). As such, we turn our attention to NAJ position where the modeled range of variability during the mid-19th to 20th centuries is found to be broadly consistent with the range exhibited by our reconstruction (Fig. 4*B*), thus supporting our suggestion that late-19th- and 20th-century NAJ variability was not unique relative to natural variability. Rather, changepoint analysis confirms that the "onset" of sustained, significant ($P < 0.05$) northward NAJ migration probably (~80% confidence) began recently within the latter half of the 20th or early 21st centuries (Fig. 4*B* and *SI Appendix*). Such delayed onset of NAJ migration—commencing nearly a century after the start of regional near-surface warming and the associated weakening of the poleward temperature gradient—appears broadly consistent with the mid-20th-century "emergence" of Atlantic-sector surface warming (5) beyond the range of natural variability.

Despite the late onset of an anthropogenic signal in the NAJ, there is a clear northward migration of the modeled NAJ during the 21st century. We thus test for the projected "emergence" of an effectively new regime of NAJ positions by probabilistically comparing NAJ position from our 13-century reconstruction to the multimodeled range of NAJ positions for each decade of the 21st century. Under our minimal mean bias adjustment and provided future high emissions (i.e., RCP8.5 and SSP5-8.5 scenarios), our results suggest that statistically significant ($P < 0.05$) differences emerge as early as 2060 CE, corresponding to a projected multimodel ensemble mean shift in the NAJ of about 0.8 to 1.0° poleward. After 2060 CE the majority (>50%) of modeled years are projected to have NAJ positions that are distinct from the probable pre-21st-century range of NAJ positions from our reconstruction. Collectively, these results greatly extend the observational context for prior model-only projections also suggesting a delayed anthropogenic emergence of NAJ changes (20, 22, 45).

When paired with our 13-century reconstruction, our proxy- and model-based results highlight that, despite a relatively late onset, unprecedented NAJ changes are projected to emerge around the mid-21st century under high emissions scenarios. As outlined herein, NAJ variability is linked to societal impacts, both positive and negative, over the past millennium. The magnitude of this natural variability, however, is significantly smaller than the changes projected by state-of-the-art models for the end of the 21st century. Although the social, political, and economic reality in which these changes will occur is different from that of the last millennium, we might expect an unprecedented poleward

shift in the NAJ to have unprecedented societal impacts. Along these lines, a poleward-shifted NAJ will directly impact future temperature and rainfall distributions across mainland Europe, with likely regional impacts that include enhanced drought and temperature extremes over southern/mainland Europe and increased pluvial frequency throughout already-wet regions of Scandinavia (22) (*SI Appendix*, Fig. S9). Such an NAJ shift will also impact the frequency and magnitude of extreme weather events across a broad portion of the Northern Hemisphere (6, 9), with potentially severe socioeconomic costs (1). By enabling insights into the range of natural NAJ variations, our results add a means of assessing the magnitude and impacts of these projected changes to the NAJ.

Materials and Methods

Climate Data Processing. We quantified the near-surface NAJ following refs. 9, 14, 16, and 20 by invoking a one-dimensional zonal-mean representation. This was done by first vertically averaging near-surface (i.e., 925- to 700-hPa levels, pressure-weighted) zonal wind speed data from the NOAA20C (23) and ERA20C (24) datasets and then zonally averaging the resultant near-surface wind speeds over the region 60°W-0°E and 15-75°N [referred to throughout as the North Atlantic zonal wind profile (16, 20)]; note that use of alternate jet stream zonal averaging regions (i.e., within ±20°) does not significantly diminish or improve reconstruction skill. Under this representation, intensity was prescribed as the maximum zonal wind speed, while position denotes the latitude of that maximum (Fig. 1). Due to the relative coarseness of both reanalysis datasets (1°), we first upscaled our North Atlantic zonal wind profile by adaptively centering a 0.001° resolution second-order polynomial fit ±5° atop the course-gridded position, following prior conventions (20). We limited our analyses of the NOAA20C and ERA20C reanalyses to the post-20th-century period (≥1900 CE), despite the former extending to 1836 CE. This truncation facilitated intercomparison of both datasets while also avoiding reliance on sparse (and potentially poor-quality) pre-20th-century meteorological measurements. During the overlapping period 1900 to 2000 CE, strongly significant ($P < 0.001$) correlations are found between position and intensity derived from the two datasets ($r_{pos.} = 0.95$; $r_{int.} = 0.94$), albeit with minor systematic mean offsets (0.4°N and 0.6 $m{\cdot}s^{-1}$).

Isotope-Enabled Climate-Model Output. For conceptual and statistical validation, we use an ensemble of water isotope ($\delta^{18}O$)-enabled global climate model simulations from the iCESM-LME, version 1.2 (26, 27). The LME incorporates a 2° atmosphere and 1° ocean version of the CESM model, run from 1 January 850 to 31 December 2005 CE. In addition to the regular hydrologic cycle, iCESM explicitly simulates the transport and transformation of water isotopes (e.g., $H_2^{18}O$) in the atmosphere, land, ocean, sea ice, and river runoff. The description of the individual isotope-enabled atmosphere, land, and ocean models is documented elsewhere (27). In this study we utilize six available ensemble members, which consist of the following transient forcings: two full-forcing runs, one greenhouse-gas-only forcing run, one orbital-only forcing run, one solar-only forcing run, and one volcanic-only forcing run. Note the only postprocessing performed on the original iCESM output was precipitation-weighted annual averaging (January to December) of the monthly fields.

Ice-Core Record Collation and Processing. We collated 29 $\delta^{18}O$ and 16 annually accumulated snowfall records from sites spanning the GrIS and its peripheral ice caps. Records were included in our compilation on the basis that each 1) be of at least annual scale resolution, 2) be well-dated (<5-y estimated uncertainty at the deepest portions of the record considered), and 3) cover at least two-thirds of, and extend beyond, the reconstruction calibration interval 1900 to 2000 CE. The period of common overlap for all 45 records is 1775 to 1967 CE, with 1 CE being the oldest year retained for preliminary analysis; all records and site diagnostics are provided in *SI Appendix*, Table S1 and can be visualized in *SI Appendix*, Fig. S3 (see also *SI Appendix*, *Proxy Record Sensitivity Analysis*).

Twenty-three out of 29 of the $\delta^{18}O$ records represent previously published data. The remaining six records (ACT11d, NU, D4, Summit2010-Composite, NEEM-2011-S1, and TUNU) represent new datasets and were analyzed at the Desert Research Institute, Reno, NV at continuous high- (≤2-cm water-equivalent) resolution following established methods (46, 47). The Summit2010-Composite record was developed by combining (via annual averaging) two adjacent cores, the Summit2010 (1743 to 2009 CE) and the Eurocore2015 records (1448 to 1763 CE; unpublished), during their period of common overlap ($P < 0.01$; $n = 21$ y). Prior to analysis, each $\delta^{18}O$ record was monthly interpolated and linearly downscaled to mean annual resolution (January to December averaging period). While prior approaches have shown promise incorporating summer-to-summer annual averages for inferring regional climatic change from Greenlandic ice-core data (48), the winter-to-winter averaging interval employed here is consistent with the majority of available, prior-published ice-core $\delta^{18}O$ and accumulation records included in our compilation (see *SI Appendix*, Table S1). The six new $\delta^{18}O$ records are on a consistent age scale, following ref. 49 prior to 1258 CE and ref. 36 thereafter.

Of the 16 accumulation records, seven records (ACT11d, ACT2, Summit2010-Composite, NEEM-2011-S1, B19, Humboldt, and TUNU) represent previously unpublished data (*SI Appendix*, Table S1). The Summit2010-Composite accumulation record was created in a fashion identical to that described for $\delta^{18}O$. All seven new records were developed at the Desert Research Institute by first identifying the depth alignment of seasonal peaks and troughs in several chemical parameters (46), permitting measurement of the (water-equivalent) thickness of the annual cycles thereafter. All seven new accumulation records are on a consistent age scale, as with the unpublished $\delta^{18}O$ records noted above (49).

NAJ Reconstruction Method. Assuming time stationarity in the underlying statistical relationships linking our GrIS ice-core compilation to the NAJ (assumptions supported by iCESM experiments; *SI Appendix*, Figs. S2 and S5) we employed a nested canonical correlation analysis–based regression to reconstruct the North Atlantic zonal wind profile across the last 13 centuries. This well-established approach was targeted specifically for its methodological compatibility with our characterization of NAJ observations, iCESM results, and proxies (Figs. 1 and 2 and *SI Appendix*, Fig. S2) and is based closely on the methodology of ref. 25. Details can be found in that study or in *SI Appendix*. Reconstruction diagnostics and sensitivity tests are outlined in *SI Appendix*, Table S2.

CMIP NAJ Projections. In order to contextualize future NAJ changes using our 13-century reconstruction, we compiled indices of NAJ position and intensity from CMIP5 and CMIP6. Due to the relatively weak response of the NAJ to late-19th-century and 20th-century anthropogenic forcing, we opted to assess here only the high-emissions scenarios, i.e., RCP8.5 [where the "8.5" denotes an average radiative forcing of +8.5 $W{\cdot}m^{-2}$ by the end of the 21st century (43)] for CMIP5 and SSP5-8.5 (where "5" denotes the "Fossil Fueled Development" future pathway for CMIP6), while retaining each corresponding "Historical" simulation. For CMIP5, 70 ensemble members were available from 30 unique models, whereas 35 CMIP6 ensemble members were available (to date) from 18 unique models, each simulating the period 1850 to 2100 CE (wherein the prescribed "Historical" period covers 1850 to 2005 CE for the CMIP5 simulations, and 1850 to 2015 CE for CMIP6). To avoid biasing our analyses toward CMIP models with numerous ensemble members (see *SI Appendix*, Table S3), we considered only the first-listed ensemble member of each model when conducting cross-model analyses (Fig. 4); we note that our results do not appreciably change when incorporating all ensemble members for each model.

Processing of the NAJ position and intensity indices was conducted in a manner identical to that described for the reanalysis data (see *Climate Data Processing*), by incorporating an adaptive second-order polynomial fit. Although there exists a wide range of spatial resolutions (0.9 to 3.3°) among models, our sensitivity analyses suggested NAJ position and intensity were generally insensitive to the details of the second-order polynomial window. At the same time, however, the CMIP models did exhibit a broad spread in mean bias and variance offsets relative to the reanalyses; model-specific biases are provided in *SI Appendix*, Table S3. Thus, in order to facilitate model reconstruction and model–model intercomparison, all CMIP-modeled position and intensity indices were mean-centered relative to the NOAA20C, to which our reconstruction is also calibrated. Critically, this conservative adjustment does not impact NAJ position and intensity variances or trends.

NAJ Migration Onset and Emergence Timing. We estimated the timing of the projected onset of NAJ migration using the significant zero crossings of derivatives (SiZer) methodology (50), in an manner identical to that recently described by ref. 5. In summary, we determined the median significant ($P < 0.05$) onset of sustained northward migration of the NAJ across all CMIP models following prefiltering of NAJ position using a range of Gaussian kernel filters incrementally distributed across 15- to 50-y bandwidths. In Fig. 4*B* we report the 95th percentile range of median values determined across all CMIP models (m = 48).

We determined the "emergence timing" by assessing the proportion of modeled years (on a per-decade basis) showing significant differences as compared to the range exhibited during the last 13 centuries of our reconstruction. In particular, we incorporated a Monte Carlo approach wherein we randomly selected with replacement m = 48 y (to match the m models) of our reconstruction. Using the resulting distributions of randomly selected position and intensity values, we then successively assessed for significant differences in the distribution of CMIP-modeled positions and intensities for each year between 1850 and 2100 CE using a one-tailed Kolmogorav–Smirnov test with a critical threshold of α = 0.05. Both steps were then repeated for a total n = 1,000 times. Finally, we assessed for the proportion of significantly different years within each decade of the 21st century, such that each decade of the 21st century resulted in one value representing the percentage of significantly different years across 10,000 tests (i.e., 10 y $\times$ 1,000 analyses). Our findings suggested that NAJ intensity is unlikely to emerge as significantly different from our reconstructed range within the forthcoming century. In contrast, the position of the NAJ under high emissions will likely become distinct (i.e., greater than 50% of years per decade with $P < 0.05$) from the range exhibited by the reconstruction by as early as 2060 CE. We note that because the range of cross-model estimated onset years and the timing of NAJ emergence was similar (within a decade) across CMIP5 and CMIP6 model estimates we opted to analyze all models together.

Data Availability. All new ice-core annual accumulation and water isotope time series presented herein, as well as NAJ reconstructions, are publicly available from the NOAA Paleoclimatology Data Archive (https://www.ncdc.noaa.gov/paleo/study/33773). NOAA20C (V3) and ERA20C U-wind and Z500 data are each available from https://www.psl.noaa.gov/data/gridded/data.20thC_ReanV3.html and https://www.ecmwf.int/en/forecasts/datasets/reanalysis-datasets/era-20c, respectively. All iCESM-LME, CMIP5, and CMIP6 U-wind, Z500, precipitation, and water isotope data are available from the NCAR Climate Data Gateway and the Earth System Grid Federation. The MATLAB code needed to reproduce the main results of this study are available at GitHub, https://github.com/mattosman/NAJ-reconstruction.

ACKNOWLEDGMENTS. We thank L. Polvani, Y. Kwan, C. Gertler, and K. Anchukaitis for useful discussions and for help in steering early versions of this manuscript. Funding for retrieval and analysis of the NU ice core was provided by the NSF Arctic System Science Program (OPP-1205196) to S.B.D. M.B.O. acknowledges support from a US Department of Defense Office of Naval Research National Defense Science and Engineering Graduate fellowship. S.C. acknowledges support from NSF award 2041281. The collection, analysis, and interpretation of the ACT11d, D4, Summit2010, Eurocore2015, NEEM-2011-S1, and Tunu2013 ice-core records were supported by NSF grants 0909541, 1023672, 1204176, and 1406219 to J.R.M. We thank all field teams and collaborators for assistance in drilling the ice cores and providing access to archived samples.

1. D. Coumou, S. Rahmstorf, A decade of weather extremes. *Nat. Clim. Chang.* **2**, 491 (2012).
2. P. D. Williams, M. M. Joshi, Intensification of winter transatlantic aviation turbulence in response to climate change. *Nat. Clim. Chang.* **3**, 644 (2013).
3. K. Chen, G. G. Gawarkiewicz, S. J. Lentz, J. M. Bane. Diagnosing the warming of the Northeastern U.S. Coastal Ocean in 2012: A linkage between the atmospheric jet stream variability and ocean response. *J. Geophys. Res.* **119**, 218–227 (2014).
4. R. Hall, R. Erdélyi, E. Hanna, J. M. Jones, A. A. Scaife. Drivers of North Atlantic Polar Front jet stream variability. *Int. J. Climatol.* **35**, 1697–1720 (2015).
5. N. J. Abram *et al*., Early onset of industrial-era warming across the oceans and continents. *Nature* **536**, 411–418 (2016).
6. V. Trouet, F. Babst, M. Meko, Recent enhanced high-summer North Atlantic Jet variability emerges from three-century context. *Nature Commun.* **9**, 180 (2018).
7. J. A. Francis, S. J. Vavrus, Evidence linking Arctic amplification to extreme weather in mid-latitudes. *Geophys. Res. Lett.* **39** (2012).
8. D. Coumou, V. Petoukhov, S. Rahmstorf, S. Petri, H. J. Schellnhuber, Quasi-resonant circulation regimes and hemispheric synchronization of extreme weather in boreal summer. *Proc. Natl. Acad. Sci.* **111**, 12331–12336 (2014).
9. T. Woollings, M. Blackburn, The North Atlantic Jet stream under climate change and its relation to the NAO and EA patterns. *J. Clim.* **25**, 886–902 (2011).
10. J. Cohen *et al*., Divergent consensuses on Arctic amplification influence on midlatitude severe winter weather. *Nat. Clim. Chang.* **10**, 20–29 (2020).
11. J. Cohen *et al*., Recent Arctic amplification and extreme mid-latitude weather. *Nat. Geosci.* **7**, 627 (2014).
12. E. A. Barnes, J. A. Screen, The impact of Arctic warming on the midlatitude jet-stream: Can it? Has it? Will it? *Wiley Interdiscip. Rev. Clim. Chang.* **6**, 277–286 (2015).
13. J. Cohen, J. Jones, Tropospheric precursors and stratospheric warmings. *J. Clim.* **24**, 6562–6572 (2011).
14. T. Woollings, C. Czuchnicki, C. Franzke, Twentieth century North Atlantic jet variability. *Q. J. Royal Meteorol. Soc.* **140**, 783–791 (2014).
15. T. Woollings *et al*., Daily to decadal modulation of jet variability. *J. Clim.* **31**, 1297–1314 (2017).
16. T. Woollings, A. Hannachi, B. Hoskins. Variability of the North Atlantic eddy-driven jet stream. *Q. J. Royal Meteorol. Soc.* **136**, 856–868 (2010).
17. B. M. Vinther, K. K. Andersen, A. W. Hansen, T. Schmith, P. D. Jones, Improving the Gibraltar/Reykjavik NAO index. *Geophys. Res. Lett.* **30**, 10.1029/2003GL018220 (2003).
18. V. Trouet *et al*., Persistent positive North Atlantic oscillation mode dominated the medieval climate anomaly. *Science* **324**, 78–80 (2009).
19. P. Ortega *et al*., A model-tested North Atlantic Oscillation reconstruction for the past millennium. *Nature* **523**, 71 (2015).
20. E. A. Barnes, L. Polvani, Response of the midlatitude jets, and of their variability, to increased greenhouse gases in the CMIP5 models. *J. Clim.* **26**, 7117–7135 (2013).
21. J. H. Yin, A consistent poleward shift of the storm tracks in simulations of 21st century climate. *Geophys. Res. Lett.* **32**, L18701 (2005).
22. C. Deser, J. W. Hurrell, A. S. Phillips, The role of the North Atlantic Oscillation in European climate projections. *Clim. Dyn.* **49**, 3141–3157 (2017).
23. G. P. Compo *et al*., The twentieth century reanalysis project. *Q. J. Royal Meteorol. Soc.* **137**, 1–28 (2011).
24. P. Poli *et al*., ERA-20C: An atmospheric reanalysis of the twentieth century. *J. Clim.* **29**, 4083–4097 (2016).
25. J. E. Smerdon, A. Kaplan, D. Chang, and M. N. Evans, A pseudoproxy evaluation of the CCA and RegEM methods for reconstructing climate fields of the last millennium. *J. Clim.* **23**, 4856–4880 (2010).
26. S. Stevenson *et al*., Volcanic eruption signatures in the isotope-enabled last millennium ensemble. *Paleoceanogr. Paleoclimatology* **34**, 1534–1552 (2019).
27. E. Brady *et al*., The connected isotopic water cycle in the Community Earth System Model version 1. *J. Adv. Model. Earth Syst.* **11**, 2547–2566 (2019).
28. J. Sjolte *et al*., Solar and volcanic forcing of North Atlantic climate inferred from a process-based reconstruction. *Clim. Past* **14**, 1179–1194 (2018).
29. L. J. Gray, T. J. Woollings, M. Andrews, J. Knight, Eleven-year solar cycle signal in the NAO and Atlantic/European blocking. *Q. J. Royal Meteorol. Soc.* **142**, 1890–1903 (2016).
30. R. Thiéblemont, K. Matthes, N.-E. Omrani, K. Kodera, F. Hansen, Solar forcing synchronizes decadal North Atlantic climate variability. *Nat. Commun.* **6**, 8268 (2015).
31. J. L. Lean, Estimating solar irradiance since 850 CE. *Earth Space Sci.* **5**, 133–149 (2018).
32. G. Chiodo, J. Oehrlein, L. M. Polvani, J. C. Fyfe, A. K. Smith. Insignificant influence of the 11-year solar cycle on the North Atlantic Oscillation. *Nat. Geosci.* **12**, 94–99 (2019).
33. J. Wang *et al*., Internal and external forcing of multidecadal Atlantic climate variability over the past 1,200 years. *Nat. Geosci.* **10**, 512 (2017).
34. I. R. Simpson, C. Deser, K. A. McKinnon, E. A. Barnes. Modeled and observed multidecadal variability in the North Atlantic jet stream and its connection to sea surface temperatures. *J. Clim.* **31**, 8313–8338 (2018).
35. S. Häkkinen, P. B. Rhines, D. L. Worthen. Atmospheric blocking and Atlantic multidecadal ocean variability. *Science* **334**, 655–659 (2011).
36. M. Sigl *et al*., Timing and climate forcing of volcanic eruptions for the past 2,500 years. *Nature* **523**, 543 (2015).
37. S. Engler, P. J. Werner, Processes prior and during the early 18th century Irish famines—Weather extremes and migration. *Climate* **3**, 1035–1056 (2015).
38. P. D. Jones, K. R. Briffa, Unusual climate in Northwest Europe during the period 1730 to 1745 based on instrumental and documentary data. *Clim. Chang.* **79**, 361–379 (2006).
39. J. Neumann, S. Lindgrén, Great historical events that were significantly affected by the weather: 4, The great famines in Finland and Estonia, 1695–97. *Bull. Am. Meteorol. Soc.* **60**, 775–787 (1979).
40. P. Slavin, Climate and famines: A historical reassessment. *WIREs Clim. Chang.* **7**, 433–447 (2016).
41. A. J. Dugmore *et al*., Cultural adaptation, compounding vulnerabilities and conjunctures in Norse Greenland. *Proc. Natl. Acad. Sci.* **109**, 3658–3663 (2012).
42. J. Olsen, N. J. Anderson, M. F. Knudsen. Variability of the North Atlantic Oscillation over the past 5,200 years. *Nat. Geosci.* **5**, 808 (2012).
43. K. E. Taylor, R. J. Stouffer, G. A. Meehl. An overview of CMIP5 and the experiment design. *Bull. Am. Meteorol. Soc.* **93**, 485–498 (2012).
44. V. Eyring *et al*., Overview of the Coupled Model Intercomparison Project Phase 6 (CMIP6) experimental design and organization. *Geosci. Model Dev.* **9**, 1937–1958 (2016).
45. C. Deser, A. Phillips, V. Bourdette, H. Teng, Uncertainty in climate change projections: The role of internal variability. *Clim. Dyn.* **38**, 527–546 (2012).
46. J. R. McConnell, G. W. Lamorey, S. W. Lambert, K. C. Taylor. Continuous ice-core chemical analyses using inductively coupled plasma mass spectrometry. *Environ. Sci. Technol.* **36**, 7–11 (2002).
47. V. Gkinis *et al*., Water isotopic ratios from a continuously melted ice core sample. *Atmos. Meas. Tech.* **4**, 2531–2542 (2011).
48. J. Sjolte *et al*., Seasonal reconstructions coupling ice core data and an isotope-enabled climate model—Methodological implications of seasonality, climate modes and selection of proxy data. *Clim. Past* **16**, 1737–1758 (2020).
49. J. R. McConnell, Pervasive Arctic lead pollution suggests substantial growth in medieval silver production modulated by plague, climate, and conflict. *Proc. Natl. Acad. Sci.* **116**, 14910–14915 (2019).
50. J. Hannig, J. S. Marron, Advanced distribution theory for SiZer. *J. Am. Stat. Assoc.* **101**, 484–499 (2006).